American Mineralogist, Volume 89, pages 785–789, 2004

The fate of structure-bound Mn^{2+} during the decomposition of dolomite and in the resulting conversion products: An EPR study

JOSEF GRANWEHR,[1,4] PETER G. WEIDLER,[2] AND ANDREAS U. GEHRING[3,*]

[1]Laboratory for Physical Chemistry, ETH Zurich, 8093 Zurich, Switzerland
[2]Forschungszentrum Karlsruhe GmbH, Institute for Technical Chemistry, Water and Geotechnology Section (ITC-WGT), D-76021 Karlsruhe, Germany
[3]Institute of Geophysics, ETH Zurich, 8093 Zurich, Switzerland
[4]Present address: Department of Chemistry, University of California, Berkeley, California 94720, U.S.A.

ABSTRACT

Dolomite from the Jhamarkotra phosphate mine (India) contains 680 ppm Mn^{2+} as indicated by electron-spin resonance spectroscopy (EPR). Dipolar broadening of the EPR signal prevents a quantitative assignment of Mn^{2+} to the Ca and Mg sites. Upon heating to 700 °C, over 99% of the dolomite is decomposed and all the Mn^{2+} is released from the dolomite structure. Approximately 95% of the original Mn^{2+} is oxidized and forms Mn-oxide. The remaining Mn^{2+} preferentially migrates into CaO. This behavior is interpreted by the Goldschmidt rule stating that smaller ions are taken up at the sites of larger ions. During subsequent hydration of CaO into $Ca(OH)_2$, the Mn^{2+} remains stable. The protection of Mn^{2+} against oxidation is explained by the topotaxical alteration of the host minerals. Carbonation of the $Ca(OH)_2$ leads to Mn^{2+} oxidation caused by the dissolution of the hydroxide prior to the formation of $CaCO_3$. Divalent Mn monitored by EPR can be used to unravel the behavior of trace elements on the molecular level during mineral alteration.

INTRODUCTION

Dolomite [$CaMg(CO_3)_2$] has a broad application in industrial production. It is used as a source of both magnesium and magnesia in concrete preparation, and in the steel industry as a flux (Oates 1998). Because of its industrial importance the physical and chemical properties, such as structure, composition, and thermal stability, have been intensively studied (e.g., Kök and Smykatz-Kloss 2001; McCauley and Johnson 1991; Haul and Wilsdorf 1952).

Dolomite often contains impurities (e.g., structure-bound trace elements), which can influence its reactivity. Little is known about the fate of these impurities during the thermal conversion into lime (CaO) and periclase (MgO). The substitution of Ca^{2+} and Mg^{2+} by Mn^{2+} is a classical example of such an impurity (Wildeman 1970; Lloyd et al. 1985; Gillhaus et al. 2000). The Mn^{2+} substitution in synthetic and natural dolomite has been characterized in several studies by electron paramagnetic resonance spectroscopy (EPR), and EPR parameters like the electron *g* matrix, the hyperfine splitting (HFS) tensor *A* or the zero-field splitting (ZFS) tensor *D* are available for Mn^{2+} at the Ca and Mg sites in dolomite (Khasanova et al. 1991; Schindler and Ghose 1970; Wildeman 1970). The separation of the two sites is only possible if the Mn^{2+} concentration is low and the paramagnetic centers are highly diluted in a diamagnetic matrix, such that they can be considered to be isolated from each other (e.g., Lumsden and Lloyd 1984). High concentrations, as are often observed in natural samples, lead to a fast relaxation of non-equilibrium magnetization and an additional broadening of homogeneous EPR lines due to an increased dipolar coupling between neighboring paramagnetic centers; thus spectral resolution is reduced (Kittel and Abrahams 1953). This renders it virtually impossible to resolve the anisotropic behavior of the above-mentioned EPR parameters. In the case of Mn^{2+}, however, the anisotropy is usually small (e.g., Zhang and Buckmaster 1993), and the spectra can be characterized reliably by determining only isotropic values of *g* and *A*.

An experimental approach based on the changes in EPR signals upon thermal and chemical treatment was developed to accurately determine the chemical environment of paramagnetic cations in multimineral systems (Gehring et al. 1999; Gehring and Karthein 1990; Angel and Vincent 1978). This approach is based on the assumption that different chemical forms or different mineral phases of a multimineral system differ in their thermal and/or chemical stability. Schosseler and Gehring (1996) expanded this approach by using pulsed EPR techniques to support the assignment of paramagnetic species. The purpose of the present research is to analyze the fate of Mn^{2+} in natural dolomite during thermal decomposition and in the resulting conversion products.

MATERIALS AND METHODS

The dolomite samples are from the Precambrian units of the Aravalli Group in Rajasthan (India) and were collected from Block B of the Jhamarkotra phosphate mine (e.g., Banerjee et al. 1980). The mineralogy of the samples was determined by X-ray powder diffraction (XRD) using a Scintag XDS 2000 equipped with a Si(Li) solid-state detector and Cu$K\alpha$ radiation in a range from $2\theta = 10$ to 65° with steps of 0.02° and counting times of 6 seconds. Quartz present in all samples was used as an internal standard for calibration of the peak positions. The XRD patterns were evaluated with the Rietveld method in order to quantify the mineral composition (Weidler et al. 1998).

For chemical analysis the dolomite samples were dissolved in a 36 M HCl solution and the Ca, Mg, Fe, and Mn concentrations were measured by atomic absorption spectrometry (AAS).

The thermal stability was evaluated using samples that had been annealed in air progressively from 100 to 800 °C for 2 hr at each step in a furnace. The samples were cooled in a desiccator and were weighed and stored under ambient laboratory

* E-mail: gehring@sl.ethz.ch

0003-004X/04/0506–785$05.00

conditions for several weeks. In addition, the annealed and aged samples were reheated at 300 °C for 4h. Mineralogical changes were analyzed by XRD.

The continuous wave (cw) X-band EPR spectra were recorded at room temperature using a Bruker ESP 300 spectrometer. The spectra were measured at a microwave (mw) frequency of 9.4 GHz with a power of 6 mW, modulation amplitude of 0.1 mT, and a modulation frequency of 100 kHz.

In addition, X-band pulse EPR experiments were used for separation and assignment of spectra composed of different components. In field-swept pulse EPR and in cw EPR experiments the signal dependence on the spin-spin or T_2 relaxation time of a sample is different (e.g., Schweiger and Jeschke 2001). The comparison of pulse and corresponding cw spectra can render possible the separation of overlapping signals. The measurements were performed with a Bruker ESP 380 spectrometer at an mw frequency of 9.76 GHz. For the field-swept two-pulse echo-detected EPR measurements the $\pi/2$ pulses were adjusted to 16 ns, the π pulses to 32 ns, and the evolution time between pulses was set to 200 ns. The sample was cooled down to 20 K.

Q-band cw EPR spectra were recorded at room temperature with a home-built spectrometer at an mw frequency of 35.26 GHz (Gromov et al. 2001). By going to higher frequency, a better resolution is obtained from samples with an anisotropic g value or of sample mixtures with unequal g values of the different components, and the field-dependent contributions to the spectrum, namely the electron and the nuclear Zeeman interaction, are better separated from the field-independent contributions like the HFS or the ZFS. Furthermore, the relative intensity of forbidden transitions is less intensive compared to allowed transitions, and higher-order effects in the spectra due to a non-spheric ligand field are reduced.

In the EPR experiments the static magnetic field was calibrated with a Bruker NMR Gaussmeter ER 035M and an XL Microwave Model 3200 frequency counter using N,N-diphenylpicrylhydrazyl (DPPH) as control marker. The Xsophe program (Hanson et al. 2001) was used to simulate the Mn^{2+} signal in dolomite in order to verify the interpretation of its half-field signal. The relative loss of the Mn^{2+} signal intensity during conversion was determined by double integration of the $m_I = \pm 5/2$ hyperfine lines in the Q-band spectra.

Results

X-ray diffraction of the untreated sample revealed dolomite as the dominant mineral phase and apatite, quartz, and calcite as minor phases. Based on peak positions, the phosphate phase could be assigned to a fluorapatite (Andreev 1994). Quantitative analysis by the Rietveld method exhibited a concentration of 91 wt% for dolomite, 8 wt% for apatite, and less than 1 wt% for quartz and calcite. The chemical composition of the dolomite sample was 33.5% CaO, 18.6% MgO, 0.4% FeO, and 0.1% Mn (680 ppm).

Based on weight loss, decomposition of the dolomite started at 600 °C and reached a maximum between 625 and 675 °C. In the sample annealed at 675 °C 21.7% dolomite was measured, at 700 °C only traces of dolomite were seen, and at 800 °C no dolomite was detected (Table 1). The newly formed phases were CaO and MgO. The latter phase remained stable during cooling and storing, whereas CaO converted to different amounts of $Ca(OH)_2$ (Table 1).

The X-band EPR spectrum of the untreated sample exhibited three groups of resonances (Fig. 1). The main lines were centered at $g \approx 2$, while weaker transitions were observed at lower field values. The spectrum around $g = 2$ showed in the vicinity of the main signal a typical pattern that could be attributed to noncentral transitions $M_S = \pm 5/2 \leftrightarrow \pm 3/2$ and $M_S = \pm 3/2 \leftrightarrow \pm 1/2$ of ^{55}Mn (100% natural abundance), which has an electron spin $S = 5/2$ and a nuclear spin $I = 5/2$ (e.g., Zhang and Buckmaster 1993). The central transitions could not be resolved conclusively due to the broad linewidth and the overlap of allowed and forbidden transitions. A better resolution was obtained in the Q-band spectrum where six dominant lines from the allowed central transitions ($M_S = +1/2 \leftrightarrow -1/2$, $\Delta m_I = 0$) were interleaved by five doublets corresponding to forbidden transitions, $\Delta M_s = \pm 1$, $\Delta m_I = \pm 1$, resulting from axial distortion of the ligand field (Mankowitz and Low 1970). The width of the six main lines, however, did not permit assignment of Mn^{2+} to the Ca and Mg sites of the dolomite, and no additional information about the Mn^{2+} distribution could be obtained.

In addition to the resonance around $g = 2$, the X-band spectrum revealed rather weak signals in the low-field range (Figs. 1 and 2). These signals could be subdivided into two different patterns, which were due to half- and third-field EPR signal of Mn^{2+}. Simulation of the low-field signal was best using EPR parameters $g = 2.0024$, $A = 9.24$ mT, and $D = 16.5$ mT for an asymmetric site, as published by Wildeman (1970) for Mn^{2+} substituting at the Mg sites in dolomite (Fig. 2).

Samples annealed at 600 °C revealed little change in intensity of the major Mn^{2+} signal. Further heating led to a drastic decrease in intensity and the generation of a new signal overlapping remains of the signal of the untreated sample. The noncentral transitions $M_S = \pm 5/2 \leftrightarrow \pm 3/2$ and $M_S = \pm 3/2 \leftrightarrow \pm 1/2$, which could be assigned to Mn^{2+} at the Mg sites in dolomite, were still detectable up to 675 °C (Fig. 3). No indication of Mn^{2+} in dolomite was found in the sample annealed at 700 °C (Fig. 4). The newly formed signal exhibited only weak forbidden transitions, and $g = 2.0015 \pm 0.0006$ and $A = 8.64 \pm 0.05$ mT parameters were determined. The hyperfine splitting is similar to the values for MgO and CaO published by Low and Offenbacher (1965). X-ray diffraction revealed these two oxides in the heated samples. The EPR spectrum showed an additional signal around $g = 2$,

Table 1. Mineral composition of the natural and treated dolomite samples determined by XRD and the Rietveld Method. All values are in weight%

T (°C)	Dolomite	Lime	Portlandite	Periclase	Apatite	Calcite
Untreated	91.2±4.3	0	0	0	8.2±1.2	<1
675	21.7±1.7	36.8±0.3	0	30.0±2.2	10.9±1.4	0
675 (aged)	19.4±1.6	0	43.5±2.3	26.9±2.0	9.8±1.2	0
675/300	18.6±1.4	0	31.2±1.4	30.4±1.0	4.4±0.9	15.1±1.1
700	1.0±0.7	48.8±0.9	0	41.5±2.2	8.1±1.3	0
700 (aged)	0.9±0.6	13.3±0.7	40.3±1.9	37.3±2.0	7.3±1.2	0
800	0	22.0±0.8	31.0±1.2	38.9±1.4	7.6±0.9	0

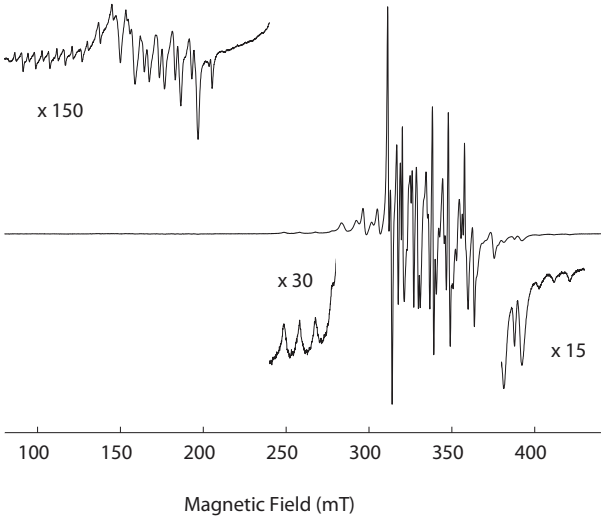

Figure 1. Wide-range X-band EPR spectrum of the untreated dolomite sample, with a blow-up of the noncentral transitions and the half and third field signals.

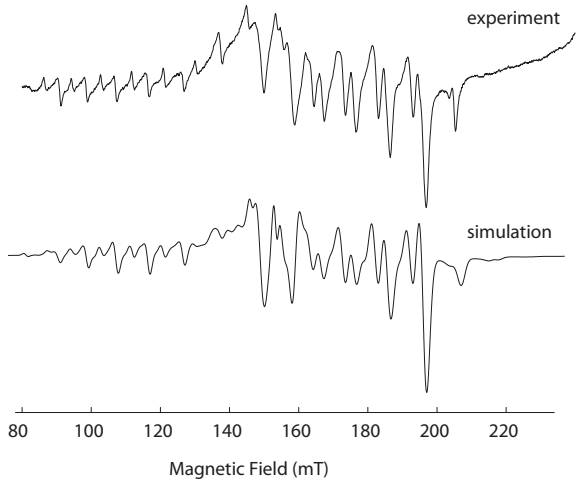

FIGURE 2. Comparison of the measured and the simulated half and third field spectra of the untreated dolomite sample.

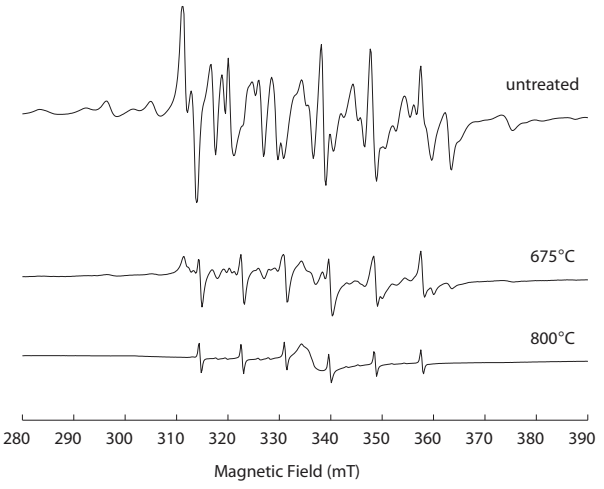

FIGURE 3. Narrow-range X-band EPR spectra of the untreated dolomite sample, and the sample after annealing at 675 and 800 °C

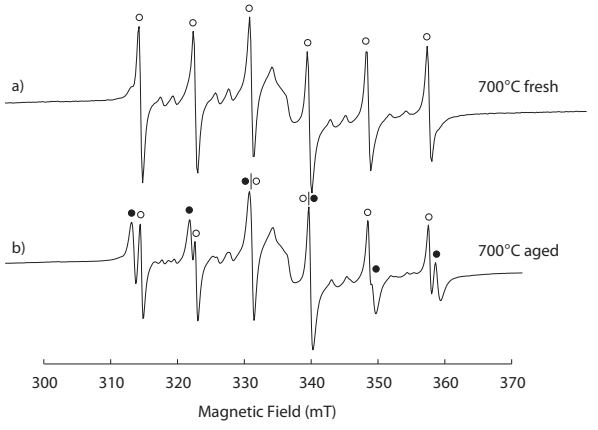

FIGURE 4. Narrow-range spectra of the sample annealed at 700 °C, cooled in the desiccator (**a**) and after aging under laboratory conditions (**b**) with Mn^{2+} in CaO/MgO (open circles) and Mn^{2+} in $Ca(OH)_2$ (filled circles).

which could be attributed to Fe^{3+} in a coordination site with high symmetry (Béltran-Lòpez and Castro-Tello 1980).

The comparison of the signal intensity of the untreated sample and the sample annealed at 800 °C showed that about 95% of the original Mn^{2+} was oxidized during decomposition of the dolomite (Fig. 3).

Storage of the thermally treated samples under ambient laboratory conditions led to spectral changes due to the generation of a new Mn^{2+} ligand field. The newly formed signal was characterized by $g = 2.0054 \pm 0.0006$ and $A = 9.08 \pm 0.06$ mT (Figs. 4 and 5a,b). These parameters are similar to those published for $Ca(OH)_2$ (e.g., Holuj et al. 1972). This phase was detected by XRD in all thermally treated samples after aging. In the sample annealed at 675 °C a complete hydration of CaO into $Ca(OH)_2$ occurred whereas in the sample annealed at 700 °C 13% of the CaO remained stable (Table 1). The latter sample exhibited after aging a superposition of the Mn^{2+} spectrum found in the fresh samples and one with EPR parameters characteristic for Mn^{2+} in $Ca(OH)_2$ (Fig. 4). In the sample annealed at 700 °C the signal attributed to Fe^{3+} revealed no change. Since this signal was stable, the comparison of the Mn^{2+} concentration of the fresh and aged samples by double integration of the spectra was possible. No significant Mn^{2+} loss was found.

Comparison of EPR spectra of the fresh and the aged sample annealed at 675 °C revealed for the aged sample the superposition of two signals arising from Mn^{2+} in $CaMg(CO_3)_2$ and in $Ca(OH)_2$ (Fig. 5). The newly formed signal attributed to Mn^{2+} in $Ca(OH)_2$ was metastable under ambient conditions. The slight changes were detected because the signal of Mn^{2+} in dolomite was stable and could, therefore, be used for calibration. The changes were nonlinear. The EPR spectra recorded after 16 and 23 weeks showed a small, but significant loss of intensity. Another 1.5 weeks later, an additional signal loss on the same order as in the previous 7 weeks was observed (Fig. 6).

Reheating the aged samples at 300 °C showed an even more drastic change in signal intensity, affecting the same signal component (Fig. 5b,c). X-ray diffractometry showed that calcite was formed at the expense of portlandite (Table 1). Subtraction of the reheated pattern from that of the aged sample revealed a six line spectrum with $g = 2.003 \pm 0.003$ and $A = 9.09 \pm 0.06$ mT, which could be assigned to Mn^{2+} in $Ca(OH)_2$ (Fig. 5d). No spectral indication for Mn^{2+} in calcite was found.

The two-pulse echo-detected EPR spectrum of the annealed sample at 675 °C after ageing consisted mainly of one Mn^{2+} component ($g = 2.002 \pm 0.003$ and $A = 9.18 \pm 0.04$ mT), which was similar to the difference spectrum attributed to $Ca(OH)_2$ (Fig. 5d,e). The narrower linewidth of the echo-detected EPR spectrum, indicating a lower Mn^{2+}concentration, could be explained by the dependence of T_2 on the distance to neighboring paramagnetic centers. Only relatively isolated Mn^{2+} might contribute to the echo. The reduced intensity of the forbidden transitions can be attributed to a different transition probability compared to allowed transitions and the fact that the pulse flip angles were adjusted for the allowed transitions (Pilbrow 1990). The corresponding cw spectrum exhibited a superposition of signals arising from Mn^{2+} in $Ca(OH)_2$ and $CaMg(CO_3)_2$. The suppres-

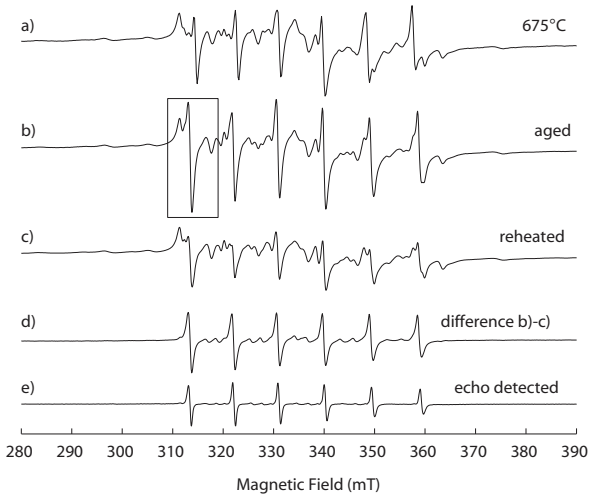

FIGURE 5. X-band cw EPR spectra of the dolomite sample annealed at 675 °C, cooled in the desiccator (**a**), after aging under laboratory conditions (**b**), and after reheating of the aged sample at 300 °C (**c**). Spectrum (**d**) is the difference between the two spectra in (**b**) and (**c**). In (**e**) the first derivative of a two-pulse echo-detected EPR spectrum of the aged sample is shown. The frame in (**b**) denotes the area shown in Figure 6.

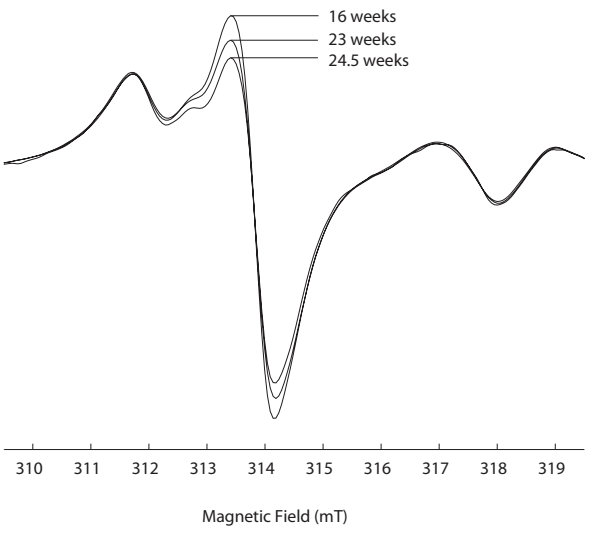

FIGURE 6. Overlay of the EPR spectra of the dolomite sample annealed at 675 °C after ageing for 16, 23, and 24.5 weeks.

sion of the latter signal from $CaMg(CO_3)_2$ in the echo-detected spectrum was caused by the higher local Mn^{2+} concentration and a corresponding reduction in T_2.

DISCUSSION

The parameters of the EPR signal of the untreated sample and their changes upon heating simultaneous to the decomposition of the dolomite argue against Mn^{2+} in apatite, which is found as the major impurity (Table 1). The broadness of the EPR signal suggests that the Mn analyzed by AAS is located in its divalent form in the dolomite structure.

Manganese(II) can substitute for Ca^{2+} as well as Mg^{2+} in the dolomite structure. The Mg-sites in contrast to the Ca-sites exhibit a distortion (Reeder and Markgraf 1986). The EPR parameters g and A obtained for Mn^{2+} at the two sites are similar. By contrast the D parameter, which is taken as a measure of the axial distortion of a crystal field from cubic symmetry, is different. The D-value for Mn^{2+} at the Ca-site is very small ($D \approx 0$ mT) and in the Mg-site is about 16 mT (e.g., Shepherd and Graham 1984; Schindler and Ghose 1970; Wildeman 1970)

The X- and Q-band EPR spectra of Precambrian dolomite reveal a superposition of the broad main lines, and, therefore, a quantitative partitioning of Mn^{2+} between the two sites is not possible. Such dipolar broadening is mainly caused by the concentration of Mn^{2+} and/or by Mn^{2+} in the presence of other paramagnetic impurities such as Fe^{3+} and has often been observed in natural dolomite samples (e.g., Lloyd et al. 1985). The presence of Mn^{2+} at the distorted Mg-sites is directly proven by the similarity of the experimental and simulated half-field spectra as well as by the occurrence of noncentral transitions. The complexity of spectrum obtained from the dolomite sample gives clues that part of the Mn^{2+} is located at the symmetric Ca-sites (cf. Lumsden and Lloyd 1984).

Since the original Mn^{2+} spectrum disappears completely upon heating to 700 °C, the temperature where only traces of dolomite was found by XRD, it can be postulated that the complete release of Mn^{2+} from the dolomite occurs simultaneously with the breakdown of this phase. The decrease of Mn^{2+} signal intensity during the decomposition of dolomite can be explained by oxidation of Mn^{2+} to Mn^{3+} and Mn^{4+}. The formation of Mn^{4+} impurities in alkaline-earth metal oxides can be ruled out since the EPR parameters are significantly different from those found in the spectra of the annealed samples (cf. Henderson and Hall 1967). Therefore, it is likely that the loss of Mn^{2+} signal is due to the formation of MnO_2. The newly formed mineral phases, lime and periclase, have cubic symmetry. It is well known that Mn^{2+} substitution can occur in both oxides (e.g., Low and Offenbacher 1965). The occurrence of weak forbidden transitions suggests a slight axial distortion of Mn^{2+}, which is due to the difference in the Me-O distance (CaO = 0.24 nm; MnO = 0.22 nm; MgO = 0.21 nm). The hyperfine splitting of $A = 8.64 \pm 0.05$ mT is similar to the values for MgO and CaO published by Low and Offenbacher (1965). The similarity of the EPR parameters does not provide an unambiguous assignment of Mn^{2+} to one of the two oxides or both of them, so far. An assignment of Mn^{2+} is possible by aging the samples, since CaO hydrates rather quickly under ambient conditions, whereas MgO is relatively inert under such conditions.

Hydration of the cubic CaO phase into the hexagonal $Ca(OH)_2$ compound results in a change of the Ca ligand field. This change is shown for Mn^{2+} substituted for Ca in the EPR spectrum of the altered sample (Figs. 4 and 5a,b). The generation of a signal characteristic of Mn^{2+} in portlandite suggests that at least a fraction of the original Mn^{2+} in dolomite incorporates into CaO during the thermal conversion. Furthermore, the fact that no significant signal loss occurs during hydration, as shown by the comparison of the Mn^{2+} spectra of the fresh and aged sample annealed at 700 °C, indicates that Mn^{2+} is in a rather stable ligand field, in which Mn^{2+} coordinated to 6 O atoms changes into a coordination with 3 O atoms and 3 OH groups. Considering the structure of lime and portlandite, the hydration can be described as a topotaxic

alteration, where the O atom layers of CaO [111] are parallel to the hydroxyl layers of $Ca(OH)_2$ [0001].

The sample annealed at 675 °C exhibits a complete hydration of CaO during aging and the simultaneously generated EPR signal reveals Mn^{2+} in $Ca(OH)_2$. Reheating leads to calcite formation at the expense of calcium hydroxide. During this conversion, by which calcium hydroxide reacts with carbon dioxide and releases water, Mn^{2+} is expelled from the structure and oxidizes. Since this reaction can proceed under ambient condition (e.g., Dheilly et al. 2002), the slight loss of signal intensity attributed to Mn^{2+} in calcium hydroxide as a consequence of ageing is explained by dissolution during carbonation.

While the periclase concentration in the fresh and aged sample annealed at 675 °C is constant, there is no persistent signal component in the various EPR spectra that corresponds to literature values for Mn^{2+} in MgO. Therefore, it can be postulated that Mn^{2+}, which withstands the thermal decomposition of dolomite, is bound in a Ca-phase. The reason why Mn^{2+} prefers sites in CaO is puzzling. An explanation for this behavior could come from the way dolomite decomposes. The thermal decomposition exhibits peculiar characteristics that depend on the atmospheric environment. It has been demonstrated that the thermal conversion under dry air occurs in two steps; first $CaCO_3$ and MgO are formed, followed by the formation of CaO at the expense of $CaCO_3$ (e.g., De Aza et al. 2002). In such a model Mg^{2+} and Ca^{2+} migrate differently. Most of Mn^{2+} reacts like the other cations and forms an oxidic phase. The remaining Mn^{2+}, however, following Goldschmidt's rule that smaller ions are taken up at the sites of larger ions, Mn^{2+} would diffuse into the Ca-phase (e.g., Kretz 1982). While no calcite was found by XRD, it can be argued that dolomite converts directly into the oxide phases or $CaCO_3$ is metastable during the annealing. Since Mn^{2+} goes along with the conversion of $CaCO_3$ into CaO (e.g., Gehring and Sposito 1995; McBride 1990) both reactions would lead to a Mn^{2+} for Ca^{2+} substitution. With this in mind, the preferential occurrence of Mn^{2+} in CaO in the annealed samples can be explained by the migration properties of Mn^{2+} and Ca^{2+} during decomposition of dolomite.

Paramagnetic Mn^{2+} is a powerful indicator to unravel the behavior of trace elements on a molecular level during thermal decomposition of natural dolomite and in the resulting products.

ACKNOWLEDGMENTS

The authors are grateful to A. Schweiger for his valuable comments on the manuscript and MTR Ltd., Udaipur, India for logistical support in the field. This research was supported by the Swiss National Science Foundation. Contribution no. 1326 Institute of Geophysics ETH Zurich.

REFERENCES CITED

Andreev, Y.G. (1994) The use of the serial-correlations concept in the figure-of-merit function for powder diffraction profile fitting. Journal of Applied Crystallography, 27, 288–297.

Angel, B.R. and Vincent, W.E.J. (1978) Electron spin resonance studies of iron oxides associated with the surface of kaolinite. Clays and Clay Minerals, 26, 263–272.

Banerjee, D.M, Basu, P.C., and Srivastava, N. (1980) Petrology, mineralogy, geochemistry, and origin of the Precambrian Aravallian phosphorite deposits of Udaipur and Jhabua, India. Economic Geology, 75, 1181–1199.

Béltran-Lòpez, V. and Castro-Tello, J. (1980) ESR lineshapes in polycrystalline samples: $^6S_{5/2}$ ions in axial and cubic crystal fields. Journal of Magnetic Resonance, 39, 437–460.

De Aza, A.H., Rodríguez, M.A., Rodríguez, J.L., De Aza, S., Pena, P., Convert, P., Hansen, T., and Turrillas, X. (2002) Decomposition of dolomite monitored by neutron thermodiffractometry. Journal of the American Ceramic Society, 85, 881–888.

Dheilly, R.M., Tudo, J., Sebai, Y., and Quéneudec, M. (2002) Influence of storage conditions on the carbonation of powdered $Ca(OH)_2$. Construction and Building Materials, 16, 155–161.

Gehring, A.U. and Karthein, R. (1990) An ESR and calorimetric study of iron oolitic samples from the Northampton ironstone. Clay Minerals, 25, 303–311.

Gehring, A.U. and Sposito, G. (1995) Residual manganese(II) speciation in montmorillonite, reply. Clays and Clay Minerals, 43, 385–386.

Gehring, A.U., Schosseler, P.M., and Weidler, P.G. (1999) Mineral formation and redox-sensitive trace elements in a near-surface hydrothermal alteration system. Geochimica et Cosmochimica Acta, 63, 2061–2069.

Gillhaus, A., Habermann, D., Meijer, J., and Richter, D.K. (2000) Cathodoluminescence spectroscopy and micro-PIXE: combined high resolution Mn-analyses in dolomites—first results. Nuclear Instruments and Methods in Physics Research Section B: Beam Interactions with Materials and Atoms, 161–163, 842–845.

Gromov, I., Shane, J., Forrer, J., Rakhmatoullin, R., Rozentzwaig, Y., and Schweiger, A. (2001) A Q-band pulse EPR/ENDOR spectrometer and the implementation of advanced one- and two-dimensional pulse EPR methodology. Journal of Magnetic Resonance, 149, 196–203.

Hanson, G.R., Noble, C.J., Gates, K.E., and Burrage, K. (2001) XSophe, a computer simulation software suite for the analysis of electron paramagnetic resonance spectra. Journal of Inorganic Biochemistry, 86, 248–248.

Haul, R.A.W. and Wilsdorf, H. (1952) Röntgenographische Untersuchung der thermischen Zersetzung von Dolomitkristallen. Acta Crystallographica, 5, 250–255.

Henderson, B. and Hall, T.P.P. (1967) Some studies of Cr^{3+} ions and Mn^{4+} ions in magnesium oxide. Proceedings of the Physical Society, 90, 511–518.

Holuj, F., Quick, M., and Roen, M. (1972) Vibronic effects in the electron paramagnetic resonance of Mn^{++} in $Ca(OH)_2$. Physical Review B, 6, 3169–3179.

Khasanova, N-M., Mukhutdinova, N.G., Nizamutdinov, N.M., Gaite, J.M., Galeev, A.A., Bulka, G.R., and Vinokurov, V.M. (1991) Indicating surface and maximal invariant components of tensor [B_{4M}] of spin-Hamiltonian of Mn^{2+} ions in crystals of calcite, magnesite, and dolomite. Soviet Physics, Crystallography, 36, 371–375.

Kittel, C. and Abrahams, E. (1953) Diolar broadening of magnetic resonance lines in magnetically diluted crystals. Physics Review, 90, 238–239.

Kök, V.M. and Smykatz-Kloss, W. (2001) Thermal characterization of dolomite. Journal of Thermal Analysis and Calorimetry, 64, 1271–1275.

Kretz, R. (1982) A model for the distribution of trace elements between calcite and dolomite. Geochimica et Cosmochimica Acta, 46, 1979–1981.

Lloyd, R.V., Lumsden, D.N., and Gregg, J.M. (1985) Relationship between paleotemperatures of metamorphic dolomites and ESR determined Mn^{2+} partitioning ratios. Geochimica et Cosmochimica Acta, 49, 2565–2568.

Low, W. and Offenbacher, E.L. (1965) Electron spin resonance of magnetic ions in complex oxides. Review of ESR results in rutile, perovskites, spinel, and garnet structures. Solid State Physics, 17, 136–216.

Lumsden, D.N. and Lloyd, R.V. (1984) Mn(II) partioning between calcium and magnesium sites in studies of dolomite origin. Geochimica et Cosmochimica Acta, 48, 1861–1865.

Mankowitz, J. and Low, W. (1970) Forbidden transition ($\Delta m = \pm 1$) in the paramagnetic resonance absorption of Mn^{2+} in calcite. Physics Review B, 2, 28–32.

McBride, M.B. (1990) Electron spin resonance. In D.L. Perry, Ed., Instrumental Surface Analysis of Geologic Materials. VCH Publisher, New York, 233–281.

McCauley, R.A. and Johnson, L.A. (1991) Decrepitation and thermal decomposition of dolomite. Thermochimica Acta, 185, 271–282.

Oates, J.A.H. (1998) Lime and Limestones: Chemistry and Technology, Production and Uses. Wiley-VCH, Weinheim.

Pilbrow, J. (1990) Transition Ion Electron Paramagnetic Resonance. Clarendon Press, Oxford.

Reeder, R.J. and Markgraf, S.A. (1986) High-temperature crystal chemistry of dolomite. American Mineralogist, 71, 795–804.

Schindler, P. and Ghose, S. (1970) Electron paramagnetic resonance of Mn^{2+} in dolomite and magnesite, and Mn^{2+} distribution in dolomites. American Mineralogist, 33, 1889–1896.

Schosseler, P.M. and Gehring, A.U. (1996) Transition metals in Llano vermiculite samples: An EPR study. Clays and Clay Minerals, 44, 70–78.

Schweiger, A. and Jeschke, G. (2001) Principles of pulse electron paramagnetic resonance. Oxford University Press, Oxford.

Shepherd, R.A. and Graham, W.R.M. (1984) EPR of Mn^{2+} in polycrystalline dolomite. Journal of Chemical Physics, 81, 6080–6084.

Weidler, P.G., Luster, J., Schneider, J., Sticher, H., and Gehring, A.U. (1998) The Rietveld method applied to the quantitative mineralogical and chemical characterization of ferralitic soils. European Journal of Soil Science, 49, 95–106.

Wildeman, T.R. (1970) The distribution of Mn^{2+} in some carbonates by electron paramagnetic resonance. Chemical Geology, 5, 167–177.

Zhang, Y.P. and Buckmaster, H.A. (1993) The 9 and 33 GHz EPR Spectra of Mn^{2+} impurity ions in polycrystalline calcite–noncentral transitions. Journal of Magnetic Resonance, Series A, 102, 151–159.

MANUSCRIPT RECEIVED JUNE 2, 2003
MANUSCRIPT ACCEPTED OCTOBER 19, 2003
MANUSCRIPT HANDLED BY DONALD ISAAK